SCIENTIFIC REPORTS

OPEN

Tunable high-order sideband spectra generation using a photonic molecule optomechanical system

Cong Cao[1], Si-Chen Mi[1], Yong-Pan Gao[1], Ling-Yan He[1], Daquan Yang[2,3], Tie-Jun Wang[1,2], Ru Zhang[1,4] & Chuan Wang[1,2]

A tunable high-order sideband spectra generation scheme is presented by using a photonic molecule optomechanical system coupled to a waveguide beyond the perturbation regime. The system is coherently driven by a two-tone laser consisting of a continuous-wave control field and a pulsed driving field which propagates through the waveguide. The frequency spectral feature of the output field is analyzed via numerical simulations, and we confirm that under the condition of intense and nanosecond pulse driving, the output spectrum exhibits the properties of high-order sideband frequency spectra. In the experimentally available parameter range, the output spectrum can be efficiently tuned by the system parameters, including the power of the driving pulse and the coupling rate between the cavities. In addition, analysis of the carrier-envelop phase-dependent effect of high-order sideband generation indicates that the system may present dependence upon the phase of the pulse. This may provide a further insight of the properties of cavity optomechanics in the nonlinear and non-perturbative regime, and may have potential applications in optical frequency comb and communication based on the optomechanical platform.

Cavity optomechanics[1,2] describes the interaction between the electromagnetic radiation and nanomechanical or micromechanical motion, which has been developing rapidly. During the past decades, it leads to various important applications, such as gravitational-wave detection[3], cooling of mechanical oscillators to the ground-state of motion[4-11], optomechanically induced transparency (OMIT) and slow light[12-18], precision measurements[19,20], squeezing of light[21], quantum information processing[22-24], and so on.

Most of the recent developments in cavity optomechanics are based on the perturbative interaction between the driving light fields and the optomechanical system. For example, in the context of OMIT, the optomechanical system is coherently driven by both a control field and a probe field. If the strength of the probe field is far less than that of the control field, the perturbation method can be used and the OMIT can be properly described by the linearization of the Heisenberg-Langevin equations. Aside from OMIT, the linearization of optomechanical interaction has also been adopted in many other studies, such as optomechanical dark state[25] and normal mode splitting[26].

One key aspect is that if the strength of the probe field becomes comparable with that of the control field, the perturbative description breaks down, and some novel nonlinear and non-perturbative effects come to appear[27,28]. Therefore, extending the studies of cavity optomechanics from the linear and perturbation regime to the nonlinear and non-perturbative regime is of great interest. On the other hand, as a natural extension of the generic optomechanical system, the composite optomechanical system which consists of two directly coupled whispering-gallery-mode microcavities (called a photonic molecule[29,30]) with optomechanical oscillation in one microcavity has attracted much attention. In the composite system, the interplay between the optomechanical interaction and the tunable photon tunnelling forms the basis of some interesting phenomena, such as phonon lasing[31,32], enhanced quantum nonlinearities[33], coherent optical wavelength conversion[34], optomechanical

[1]School of Science, Beijing University of Posts and Telecommunications, Beijing 100876, China. [2]State Key Laboratory of Information Photonics and Optical Communications, Beijing University of Posts and Telecommunications, Beijing 100876, China. [3]School of Information and Communication Engineering, Beijing University of Posts and Telecommunications, Beijing 100876, China. [4]School of Ethnic Minority Education, Beijing University of Posts and Telecommunications, Beijing 100876, China. Correspondence and requests for materials should be addressed to C.W. (email: wangchuan@bupt.edu.cn)
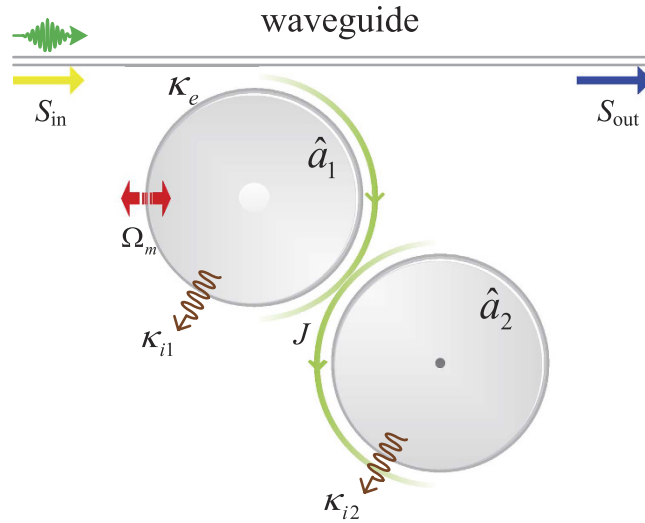
Figure 1. Schematic diagram of a double-cavity photonic molecule optomechanical system coupled to a waveguide. S_{in} (S_{out}) represents the input (output) field propagating in the waveguide. $\hat{a}_1$ ($\hat{a}_2$) denotes the bosonic annihilation operator of the first (second) cavity field. The first cavity supports a mechanical mode with angular frequency Ω_m. J is the cavity-cavity coupling rate, which can be efficiently adjusted by the distance between the cavities. κ_e denotes the coupling rate between the first cavity and the waveguide. κ_{i1} and κ_{i2} are the intrinsic cavity decay rates.

quantum gates[22,23], coherent control of light transmission[35–41], chaos[42], and ground-state cooling of mechanical modes[43,44].

In this work, we investigate the tunable high-order sideband spectra generation using a photonic molecule optomechanical system coupled to a waveguide in the non-perturbation regime. The composite system is coherently driven by a two-tone laser consisting of a continuous-wave (CW) control field and a pulsed driving field which propagates through the waveguide. We analyze the frequency spectral feature of the output field by performing fast Fourier transformation (FFT), and confirm that under the condition of intense and nanosecond pulse driving, the output spectrum exhibits the properties of high-order sideband frequency spectra. We find that the output spectrum can be efficiently tuned by using the power of the driving pulse and the coupling rate between the cavities. In addition, we show the carrier-envelop phase-dependent (CEP-dependent) effect of high-order sideband generation in the output spectra, and the results indicate that the CEP of laser pulse which contains huge numbers of cycles can also cause profound effects. Our study may provide a further insight of the properties of cavity optomechanics in the nonlinear and non-perturbative regime, and may have potential applications in optical frequency comb and communication based on the optomechanical platform[45]. Also the proposed whispering-gallery-mode photonic molecule-waveguide structure is compatible with large-scale integration for implementing complex photonic devices on a chip.

Results

Model. As shown in Fig. 1, we consider a system of two directly coupled whispering-gallery-mode microcavities. The first cavity with an effective mass m supports an optical mode $\hat{a}_1$ and a mechanical mode with angular frequency Ω_m. The second cavity only supports an optical mode $\hat{a}_2$ which is coupled to the first cavity through an evanescent field. The cavity-cavity coupling rate J can be efficiently tuned by changing the distance between them. A tapered fiber is used to excite the cavity modes as the optical waveguide. The first cavity is side coupled to the fiber with the coupling rate κ_e. S_{in} and S_{out} represent the input and the output fields propagating in the waveguide, respectively. The Hamiltonian of this composite system can be divided into three parts, i.e.,

$$\hat{H} = \hat{H}_0 + \hat{H}_{\text{int}} + \hat{H}_{dr}, \tag{1}$$

where $\hat{H}_0$, $\hat{H}_{\text{int}}$ and $\hat{H}_{dr}$ are the free Hamiltonian, interaction Hamiltonian and the driven Hamiltonian, respectively, which can be written as

$$
\begin{aligned}
\hat{H}_0 &= \hbar\omega_c\hat{a}_1^\dagger\hat{a}_1 + \hbar\omega_c\hat{a}_2^\dagger\hat{a}_2 + \frac{\hat{p}^2}{2m} + \frac{1}{2}m\Omega_m^2\hat{x}^2, \\
\hat{H}_{\text{int}} &= -\hbar J(\hat{a}_1^\dagger\hat{a}_2 + \hat{a}_2^\dagger\hat{a}_1) - \hbar G\hat{x}\hat{a}_1^\dagger\hat{a}_1, \\
\hat{H}_{dr} &= i\hbar\sqrt{\kappa_e}(\hat{a}_1^\dagger S_{in} - \hat{a}_1 S_{in}^*),
\end{aligned}
\tag{2}
$$

where $\hat{a}_{1(2)}$ and $\hat{a}_{1(2)}^\dagger$ represent the bosonic annihilation and creation operators of the first (second) cavity mode. ω_c is the resonance frequency of the two cavities. $\hat{x}$ and $\hat{p}$ denote the mechanical position and momentum operators. G is the optomechanical coupling constant. Here we focus on the mean response of the composite system.
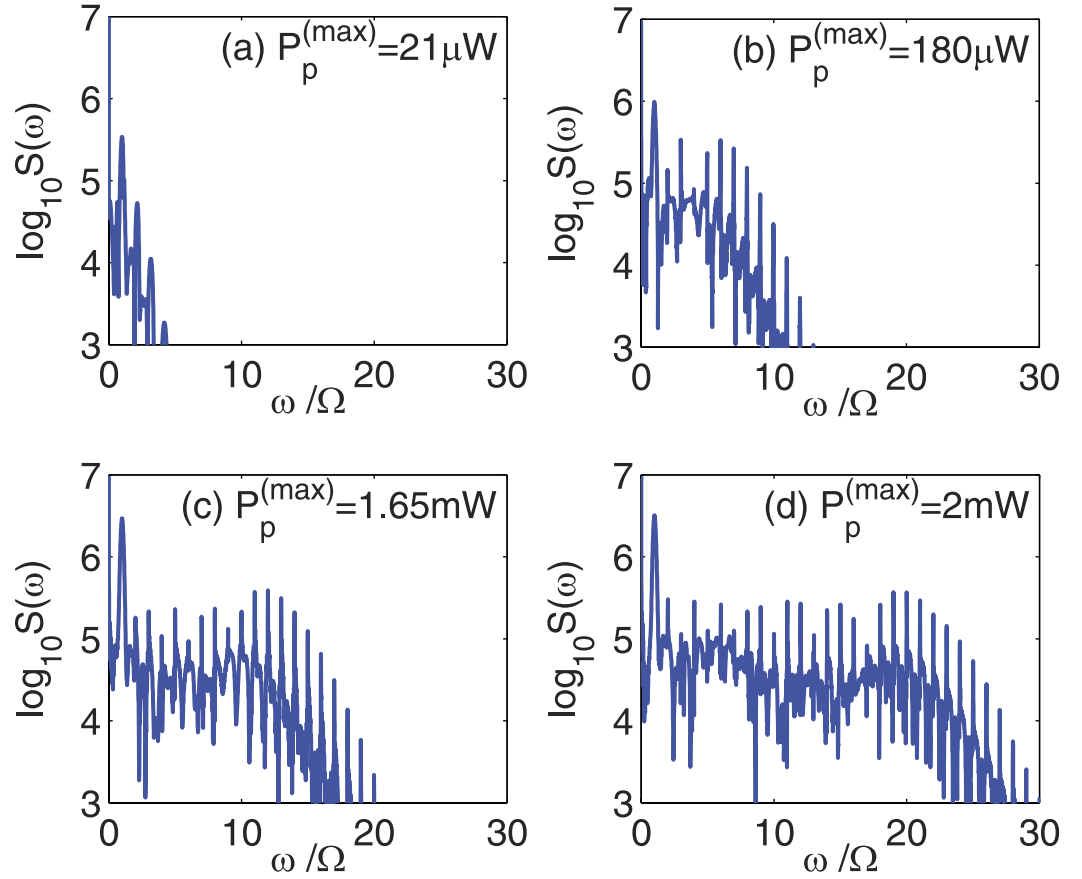
Figure 2. Frequency spectra of the output field with different values of $P_p^{(max)}$ as: (**a**) $P_p^{(max)} = 21\,\mu W$, (**b**) $P_p^{(max)} = 180\,\mu W$, (**c**) $P_p^{(max)} = 1.65\,mW$, and (**d**) $P_p^{(max)} = 2\,mW$. Here the CW control field has wavelength 532 nm and power $P_1 = 37.3\,\mu W$. The driving pulse has center time $t_0 = 0.2\,\mu s$, FWHM $t_p = 12\,ns$, and CEP $\phi = 0$. The cavity-cavity coupling rate is $J = 2\pi \times 0.5\,MHz$. The other system parameters used for calculations are $\kappa_e = 2\pi \times 45.5\,MHz$, $\kappa_{i1} = \kappa_{i2} = 2\pi \times 0.5\,MHz$, $m = 2.0\,pg$, $\Omega_m = 1.4\,GHz$, $\Gamma_m = 2\pi \times 35\,kHz$, $G = 485.0\,GHz/nm$, and $\Delta = -\Omega_m$, respectively.

Assuming $\langle \hat{a}_1(t) \rangle = a_1(t)$, $\langle \hat{a}_1^\dagger(t) \rangle = a_1^*(t)$, $\langle \hat{a}_2(t) \rangle = a_2(t)$, $\langle \hat{x}(t) \rangle = x(t)$, $\langle \hat{p}(t) \rangle = p(t)$, and by using the mean-field approximation $\langle \hat{A}\hat{B} \rangle = \langle \hat{A} \rangle \langle \hat{B} \rangle$, the Heisenberg-Langevin equations of the operators can be reduced to the mean value equations as:

$$\dot{a}_1 = \left(-i\omega_c + iGx - \frac{\kappa_e}{2} - \frac{\kappa_{i1}}{2} \right) a_1 \\ + iJa_2 + \sqrt{\kappa_e}S_{in},$$

(3)

$$\dot{a}_2 = \left(-i\omega_c - \frac{\kappa_{i2}}{2} \right) a_2 + iJa_1,$$

(4)

$$\dot{x} = \frac{p}{m},$$

(5)

$$\dot{p} = -m\Omega_m^2 x + \hbar G a_1^* a_1 - \Gamma_m p,$$

(6)

where κ_{i1} and κ_{i2} are the cavity intrinsic decay rates. Γ_m represents the mechanical decay rate, which is introduced classically. The quantum and thermal noise terms are dropped as their mean values are 0. Eqs (3)–(6) are coupled ordinary differential equations of complex functions which describe the time evolution of the composite system.

In the following, we consider the case that the input field contains a CW control field and a pulsed driving field, i.e., $S_{in}(t) = s_1 e^{-i\omega_1 t} + s_p \varepsilon(t) e^{-i(\omega_p t + \phi)}$. s_1 and $s_p \varepsilon(t)$ are the amplitudes of the two fields, which are related to the optical powers propagating in the waveguide by $P_1 = \hbar \omega_1 s_1^2$ and $P_p(t) = \hbar \omega_p s_p^2 \varepsilon^2(t)$, respectively. ω_1 and ω_p are the frequency of the control field and the mean frequency of the driving pulse, respectively. $\varepsilon(t)$ is the
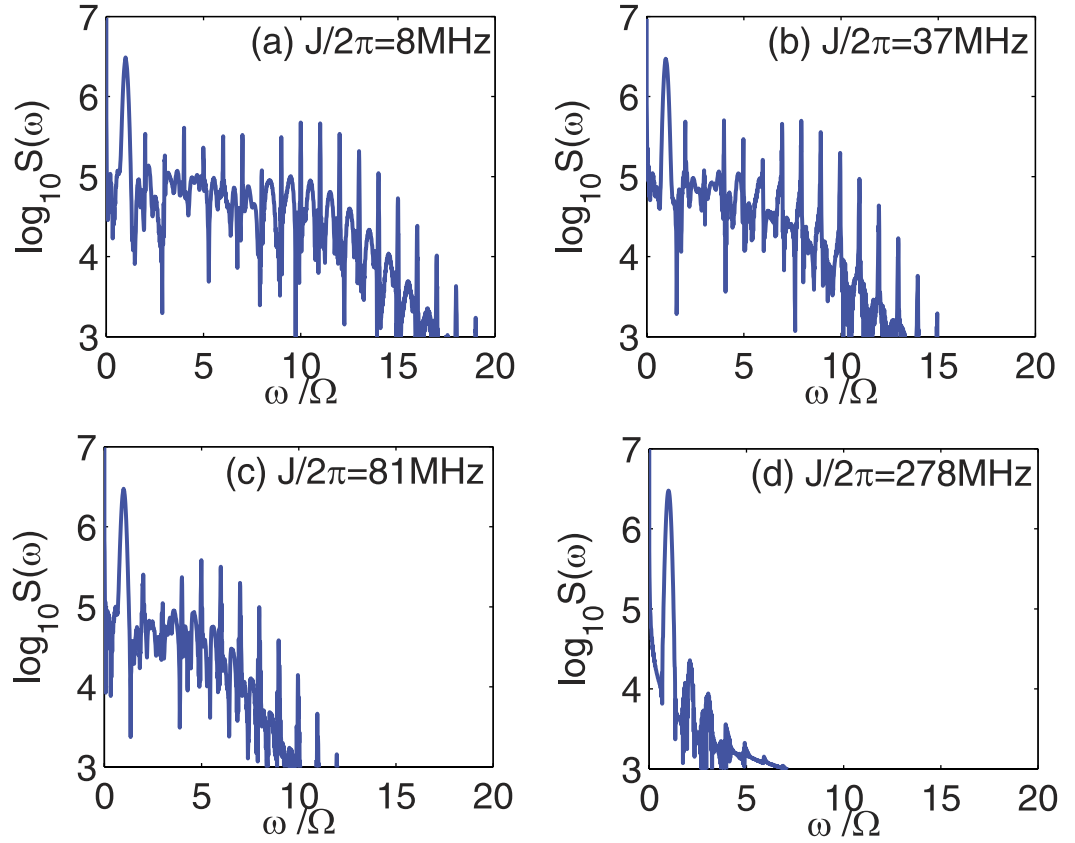
Figure 3. Frequency spectra of the output field with different values of J as: (**a**) $J = 2\pi \times 8\,\text{MHz}$, (**b**) $J = 2\pi \times 37\,\text{MHz}$, (**c**) $J = 2\pi \times 81\,\text{MHz}$, and (**d**) $J = 2\pi \times 278\,\text{MHz}$. Here the power of the CW control field is $P_1 = 37.3\,\mu\text{W}$, the maximum power of the driving pulse is $P_p^{(\text{max})} = 1.65\,\text{mW}$, and the other parameters are the same as in Fig. 2.

normalized pulse envelope which is assumed to be Gaussian here, i.e., $\varepsilon(t) = \exp[-2\ln 2(t-t_0)^2/t_p^2]$, with t_0 being the center time of the pulse and t_p being the full width of half maximum (FWHM) of the intensity envelop. ϕ is the so-called CEP of the driving pulse. In this case, the maximum power of the driving pulse is $P_p^{(\text{max})} = \hbar\omega_p s_p^2$. In a rotating frame at the frequency of ω_1, the evolution equations of the composite system can be rewritten as:

$$\dot{a}_1 = \left(i\Delta + iGx - \frac{\kappa_e}{2} - \frac{\kappa_{i1}}{2}\right)a_1 + iJa_2$$
$$+ \sqrt{\kappa_e}[s_1 + s_p\varepsilon(t)e^{-i(\Omega t + \phi)}], \tag{7}$$

$$\dot{a}_2 = \left(i\Delta - \frac{\kappa_{i2}}{2}\right)a_2 + iJa_1, \tag{8}$$

$$\dot{x} = \frac{p}{m}, \tag{9}$$

$$\dot{p} = -m\Omega_m^2 x + \hbar Ga_1^* a_1 - \Gamma_m p, \tag{10}$$

where $\Delta = \omega_1 - \omega_c$ is the detuning between the frequency of the control field ω_1 and the cavity resonance frequency ω_c. $\Omega = \omega_p - \omega_1$ is the detuning between the mean frequency of the driving pulse ω_p and the frequency of the control field ω_1. In such a rotating frame, $s_1 + s_p\varepsilon(t)e^{-i(\Omega t + \phi)}$ can be seen as the effective input field, and the mean frequency of the effective driving pulse becomes Ω. Here, we set Ω equals to the low-frequency mechanical mode Ω_m, which has been widely employed in OMIT.

High-order sideband frequency spectra generation. Figure 2 shows the frequency spectra of the output field with different powers of the driving pulse $P_p^{(\text{max})}$ as: (a) $P_p^{(\text{max})} = 21\,\mu\text{W}$, (b) $P_p^{(\text{max})} = 180\,\mu\text{W}$, (c) $P_p^{(\text{max})} = 1.65\,\text{mW}$, and (d) $P_p^{(\text{max})} = 2\,\text{mW}$. Here the CW control field has wavelength 532 nm and power
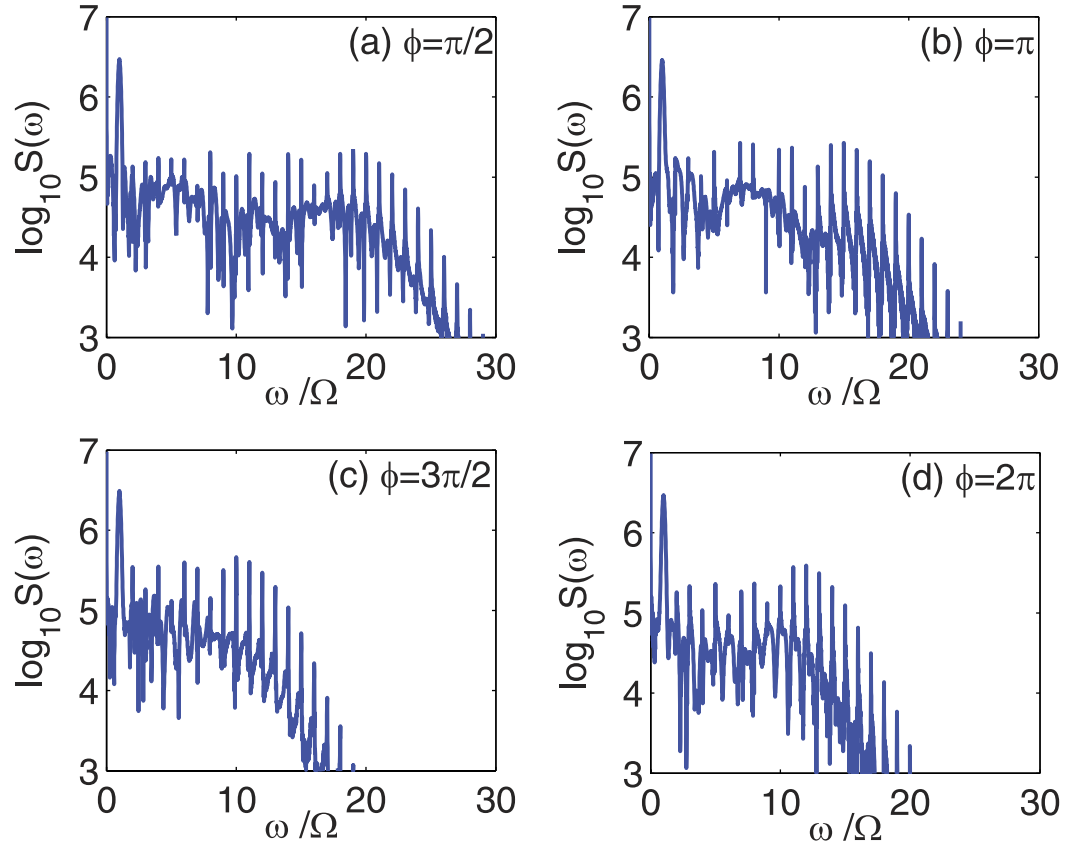
Figure 4. Frequency spectra of the output field with different values of ϕ as: (**a**) $\phi = \pi/2$, (**b**) $\phi = \pi$, (**c**) $\phi = 3\pi/2$, and (**d**) $\phi = 2\pi$. Here we use $P_1 = 37.3\,\mu\text{W}$, $P_P^{(\text{max})} = 1.65\,\text{mW}$, and the other parameters are the same as in Fig. 2.

$P_1 = 37.3\,\mu\text{W}$, with $\Delta = -\Omega_m$. The driving pulse has center time $t_0 = 0.2\,\mu\text{s}$, FWHM $t_p = 12\,\text{ns}$, and CEP $\phi = 0$. The cavity-cavity coupling rate is $J = 2\pi \times 0.5\,\text{MHz}$. As the Eqs (7)–(10) describe the evolution of the optical fields in a frame rotating at the frequency ω_1, the output spectra exhibit a frequency shift of ω_1. Moreover, there are positive frequencies and negative frequencies during FFT, and we only show the positive frequency components here. From Fig. 2, one can see that the output spectra contain two input field frequency components (the CW control field ω_1 and the pulsed driving field $\omega_p = \omega_1 + \Omega$), and a series of new components (higher-order sidebands). That is, when the driving pulse is incident upon the composite system which has been driven by the CW control field, the spectral components with frequencies $\omega = \omega_1 \pm n\Omega$ can be generated in the output field, where $n = 0,1,2,\ldots$ represents the order of the sidebands. When the driving pulse is relatively weak, e.g., $P_p^{(\text{max})} = 21\,\mu\text{W}$ in Fig. 2(a), there are only a few sidebands appear in the spectrum, and the intensity of individual sideband is decreased rapidly as the order of the sidebands is increased. As the power of the driving pulse is increased, e.g., $P_p^{(\text{max})} = 180\,\mu\text{W}$ in Fig. 2(b) and $P_p^{(\text{max})} = 1.65\,\text{mW}$ in Fig. 2(c), the effect of high-order sideband generation could be observed. When the pulse power is sufficiently high, e.g., $P_p^{(\text{max})} = 2\,\text{mW}$ in Fig. 2(d), a robust high-order sideband generation can be achieved. In this case, the spectrum decreases rapidly for the first few order sidebands, followed by a plateau where the sideband intensity is slowly varying, and ends up with a sharp cutoff. Such typical spectral feature indicates the non-perturbative nature of high-order sideband generation[27], which is very similar to the high-order harmonic generation in strongly driven atoms or molecules[46,47].

In experiment, the cavity-cavity coupling rate J can be efficiently adjusted by changing the distance between the cavities. In order to show the influence of the parameter J on the high-order sideband spectra generation, Fig. 3 shows the frequency spectra of the output field with different values of J as: (a) $J = 2\pi \times 8\,\text{MHz}$, (b) $J = 2\pi \times 37\,\text{MHz}$, (c) $J = 2\pi \times 81\,\text{MHz}$, and (d) $J = 2\pi \times 278\,\text{MHz}$. Note that the power of the CW control field is $P_1 = 37.3\,\mu\text{W}$, the maximum power of the driving pulse is $P_p^{(\text{max})} = 1.65\,\text{mW}$, and the other system parameters used for calculations are the same as in Fig. 2. When J is relatively small, e.g., $J = 2\pi \times 8\,\text{MHz}$ in Fig. 3(a), a lot of high-order sidebands can be obtained and the corresponding sideband intensities are large. With the increment of J, e.g., $J = 2\pi \times 37\,\text{MHz}$ in Fig. 3(b) and $J = 2\pi \times 81\,\text{MHz}$ in Fig. 3(c), the intricate competition between the two kinds of couplings, i.e., the cavity-cavity coupling and the optomechanical coupling, becomes obvious. Due to the linear cavity-cavity coupling indirectly influences the optomechanical coupling strength, the nonlinear effect of high-order sideband generation is decreased[48,49]. Last, for a large J, e.g., $J = 2\pi \times 278\,\text{MHz}$ in Fig. 3(d), the photon tunnelling between the two cavities dominates the evolution process. As a result, only a few sidebands appear in the spectrum and the intensity of individual sideband is decreased rapidly as the sideband order is increased. This
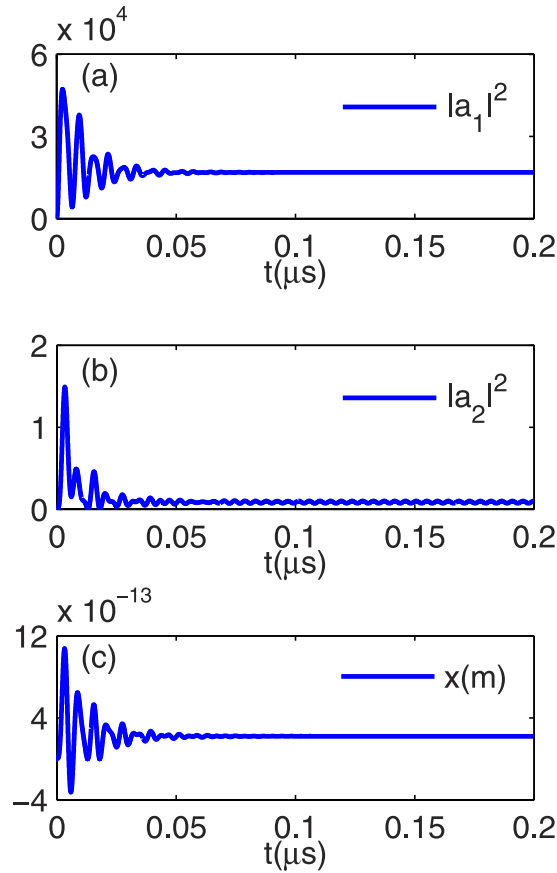
Figure 5. Intensities of the optical fields and the mechanical oscillation in time domain by directly solving Eqs (7)–(10) with $s_p = 0$ and $J = 2\pi \times 0.5$ MHz. The time evolution of the (**a**) photon number in the first cavity $|a_1|^2$, (**b**) photon number in the second cavity $|a_2|^2$, and (**c**) mechanical position x in 0.2 μs are shown.

phenomenon provides us a potentially useful method to tune the output spectrum by using the photon tunnelling of the coupled cavities.

On the other hand, the CEP is another key parameter in describing the characteristics of the driving pulse. According to Eqs (7)–(10), when the CEP of the driving pulse ϕ goes to $\phi + 2\pi$, the time evolution of the composite system remains unchanged. Thus there is a periodicity upon the CEP, where ϕ goes to $\phi + 2\pi$ leads to the same output spectra. However, within a range of 2π, the spectra may also be different for different values of ϕ. Figure 4 shows such a CEP-dependent effect of high-order sideband generation with different values of ϕ as: (a) $\phi = \pi/2$, (b) $\phi = \pi$, (c) $\phi = 3\pi/2$, and (d) $\phi = 2\pi$. Here we use $P_1 = 37.3 \mu$W, $P_P^{(max)} = 1.65$ mW, and the other parameters are the same as in Fig. 2. Usually, the CEP only strongly affects the processes involving few-cycle light pulses[50,51]. For $t_p = 12$ ns, the number of cycles in the driving pulse can be estimated to be $2t_p\omega_p/2\pi \sim 10^7$, which means the driving pulse contains huge numbers of cycles and seems almost impossible to have the CEP-dependent effects. However, the dynamics of the composite system in our scheme is in a rotating frame, the mean frequency of the effective driving pulse is Ω, which equals to the low-frequency mechanical mode Ω_m. One can estimate the number of cycles in the effective driving pulse to be $2t_p\Omega/2\pi \sim 6$ by choosing $t_p = 12$ ns and $\Omega = 1.4$ GHz, which means the effective driving pulse only contains a few cycles. We can conclude that the CEP of the driving pulse becomes important and can produce obvious influences on the output spectra, even though the driving pulse contains huge numbers of cycles in reality. For longer driving pulses, the influence of the CEP on high-order sideband generation would become smaller[49].

Before ending, it is worth emphasizing that the linewidth of the high-order sidebands can be well described by the time-frequency uncertainty relation $\Delta\omega\Delta t \sim 2\pi$[27,28,48,49]. In our scheme, the driving pulse lasts about $2t_p$, so $\Delta t \approx 2t_p$. Making use of the relationship $\Delta\omega \sim 2\pi/\Delta t$, we can roughly estimate the linewidth of the generated high-order sidebands to be $\Delta\omega \sim \Omega_m/5$. Therefore, the high-order sidebands are relatively narrow and clearly resolved in the spectra.

Summary
In summary, we have theoretically and numerically analyzed the nonlinear optical transmission characteristics in a waveguide-coupled photonic molecule optomechanical system. The composite system is coherently driven by a CW control field and an intense nanosecond driving pulse, and the numerical method is employed instead of the perturbation method in such a non-perturbative regime. By performing FFT, the frequency spectrum of

the output field of the system can be obtained. We confirmed that the output spectrum exhibits the properties of high-order sideband frequency spectra, and the typical spectral feature reveals the non-perturbative nature of high-order sideband generation. The results clearly show that the output spectrum is tunable by changing the power of the driving pulse and also by using the photon tunnelling of the coupled cavities. In addition, we investigated the CEP-dependent effect of high-order sideband generation in the output spectra. The results may have potential applications in optical frequency comb and communication based on the optomechanical platform, and may open up a promising perspective for implementing complex photonic devices on a chip.

Method

In order to show the non-perturbative signals explicitly, we directly solved the evolution equations to study the dynamics of the system. The Runge-Kutta method is employed and the initial conditions are set as: $a_1(0) = 0$, $a_2(0) = 0$, $x(0) = 0$, and $p(0) = 0$, which can be achieved by cooling the mechanical mode to the ground-state of motion. The relevant system parameters used for calculations are $\kappa_e = 2\pi \times 45.5$ MHz, $\kappa_{i1} = \kappa_{i2} = 2\pi \times 0.5$ MHz, $m = 2.0$ pg, $\Omega_m = 1.4$ GHz, $G = 485.0$ GHz/nm, $\Gamma_m = 2\pi \times 35$ kHz, and $\Delta = -\Omega_m$, respectively. All these parameters are within the experimentally available parameter range[52], and are used through out the paper.

Firstly, we consider $s_p = 0$ and only a CW control field with wavelength 532 nm and power $P_1 = 37.3$ µW is incident upon the composite system. In this case, the system would evolve to a steady state provided by the effective field s_1. Figure 5 shows the time evolution of the composite system by solving Eqs (7)–(10) with the numerical method. One can see that after a transient process, the system reaches the steady state at about $t = 0.1$ µs.

Next, the input field contains a CW control field and a nanosecond driving pulse is taken into consideration. The center time of the driving pulse is adjusted to $t_0 = 0.2$ µs to make sure that when the pulse is incident upon the composite system, the system has reached the steady state. The output field transmitting through the waveguide can be obtained by using the standard input-output formalism as $S_{out}(t) = S_{in}(t) - \sqrt{\kappa_e} a_1(t)$. The output spectrum $S(\omega) \propto |\int_{-\infty}^{+\infty} S_{out}(t) e^{-i\omega t} dt|$ can be numerically obtained by performing FFT on $S_{out}(t)$, where ω is the spectrometer frequency. Here we do the FFT from $t = 0.15$ µs which is after the composite system reaches the steady state and before the driving pulse is incident upon the composite system, so that the complicated transient process has no influence on the spectral characters.

References

1. Kippenber, T. J. & Vahala, K. J. Cavity opto-mechanics. *Opt. Express* **15**, 17172–17205 (2007).
2. Aspelmeyer, M., Kippenberg, T. J. & Marquardt, F. Cavity optomechanics. *Rev. Mod. Phys.* **86**, 1391–1452 (2014).
3. Buonanno, A. & Chen, Y. Scaling law in signal recycled laser-interferometer gravitational-wave detectors. *Phys. Rev. D* **67**, 062002 (2003).
4. Marquardt, F., Chen, J. P., Clerk, A. A. & Girvin, S. M. Quantum theory of cavity-assisted sideband cooling of mechanical motion. *Phys. Rev. Lett.* **99**, 093902 (2007).
5. Li, Y., Wu, L. A., Wang, Y. D. & Yang, L. P. Nondeterministic ultrafast ground-state cooling of a mechanical resonator. *Phys. Rev. B* **84**, 094502 (2011).
6. Liu Y. C., Xiao Y. F., Luan X. & Wong C. W. Dynamic dissipative cooling of a mechanical resonator in strong coupling optomechanics. *Phys. Rev. Lett.* **110(15)**, 153606 (2013).
7. Zhu, J. & Li, G. Ground-state cooling of a nanomechanical resonator with a triple quantum dot via quantum interference. *Phys. Rev. A* **86**, 053828 (2012).
8. Yi, Z., Gu, W. J. & Li, G. Sideband cooling of atoms with the help of an auxiliary transition. *Phys. Rev. A* **86**, 055401 (2012).
9. Gu, W. J. & Li, G. Quantum interference effects on ground-state optomechanical cooling. *Phys. Rev. A* **87**, 025804 (2013).
10. Liu Y. C., Xiao, Y. F., Luan, X., Gong, Q. H. & Wong C. W. Coupled cavities for motional ground-state cooling and strong optomechanical coupling. *Phys. Rev. A* **91(3)**, 033818 (2015).
11. Liu Y. C., Hu, Y. -W., Wong, C. W. & Xiao, Y. F. Review of cavity optomechanical cooling. *Chin. Phys. B* **22(11)**, 114213 (2013).
12. Agarwal, G. S. & Huang, S. Electromagnetically induced transparency in mechanical effects of light. *Phys. Rev. A* **81**, 041803 (2010).
13. Weis, S. *et al.* Optomechanically induced transparency. *Science* **330**, 1520–1523 (2010).
14. Khurgin, J. B., Pruessner, M. W., Stievater, T. H. & Rabinovich, W. S. Laser-rate-equation Ddescription of optomechanical oscillators. *Phys. Rev. Lett.* **108**, 223904 (2012).
15. Verhagen, E., Deléglise, S., Weis, S., Schliesser, A. & Kippenberg, T. J. Quantum-coherent coupling of a mechanical oscillator to an optical cavity mode. *Nature* **482**, 63–67 (2012).
16. Xiong, H., Si, L. G., Zheng, A. S., Yang, X. & Wu, Y. Higher-order sidebands in optomechanically induced transparency. *Phys. Rev. A* **86**, 013815 (2012).
17. Karuza, M. *et al.* Optomechanically induced transparency in a membrane-in-the-middle setup at room temperature. *Phys. Rev. A* **88**, 013804 (2013).
18. Chang, D. E., Safavi-Naeini, A. H., Hafezi, M. & Painter, O. Slowing and stopping light using an optomechanical crystal array. *New J. Phys.* **13**, 023003 (2011).
19. Zhang, J. Q., Li, Y., Feng, M. & Xu, Y. Precision measurement of electrical charge with optomechanically induced transparency. *Phys. Rev. A* **86**, 053806 (2012).
20. Wang, Q., Zhang, J. Q., Ma, P. C., Yao, C. M. & Feng, M. Precision measurement of the environmental temperature by tunable double optomechanically induced transparency with a squeezed field. *Phys. Rev. A* **91**, 063827 (2015).
21. Purdy, T. P., Yu, P.-L., Peterson, R. W., Kampel, N. S. & Regal, C. A. Strong optomechanical squeezing of light. *Phys. Rev. X* **3**, 031012 (2013).
22. Stannigel, K. *et al.* Optomechanical quantum information processing with photons and phonons. *Phys. Rev. Lett.* **109**, 013603 (2012).
23. Komar, P. *et al.* Single-photon nonlinearities in two-mode optomechanics. *Phys. Rev. A* **87**, 013839 (2013).
24. Rips, S. & Hartmann, M. J. Quantum information processing with nanomechanical qubits. *Phys. Rev. Lett.* **110**, 120503 (2013).
25. Dong, C., Fiore, V., Kuzyk, M. C. & Wang, H. Optomechanical dark mode. *Science* **338**, 1609–1613 (2012).
26. Ma, J. *et al.* Optomechanically induced transparency in the mechanical-mode splitting regime. *Opt Lett.* **39**, 4180–4183 (2014).
27. Xiong, H., Si, L. G., Lü, X. Y., Yang, X. X. & Wu, Y. Carrier-envelope phase-dependent effect of high-order sideband generation in ultrafast driven optomechanical system. *Opt. Lett.* **38**, 353–355 (2013).
28. Xiong, H., Si, L. G., Lü, X. Y., Yang, X. X. & Wu, Y. Nanosecond-pulse-controlled higher-order sideband comb in a GaAs optomechanical disk resonator in the non-perturbative regime. *Ann. Phys.* **349**, 43–54 (2014).

29. llchenko, V. S., Gorodetsky, M. L. & Vyatchanin, S. P. Coupling and tunability of optical whispering-gallery modes: a basis for coordinate meter. *Opt. Commun.* **107,** 41–48 (1994).
30. Peng, B., Özdemir, S. K., Zhu, J. & Yang, L. Photonic molecules formed by coupled hybrid resonators. *Opt. Lett.* **37,** 3435–3437 (2012).
31. Grudinin, I. S., Lee, H., Painter, O. & Vahala, K. J. Phonon laser action in a tunable two-level system. *Phys. Rev. Lett.* **104,** 083901 (2010).
32. Jing, H. *et al.* PT-symmetric phonon laser. *Phys. Rev. Lett.* **113,** 053604 (2014).
33. Ludwig, M., Safavi-Naeini, A. H., Painter, O. & Marquardt, F. Enhanced quantum nonlinearities in a two-mode optomechanical system. *Phys. Rev. Lett.* **109,** 063601 (2012).
34. Hill, J. T., Safavi-Naeini, A. H., Chan, J. & Painter, O. Coherent optical wavelength conversion via cavity optomechanics. *Nat. Commun.* **3,** 1196 (2012).
35. Qu, K. & Agarwal, G. S. Phonon-mediated electromagnetically induced absorption in hybrid opto-electromechanical systems, *Phys. Rev. A* **87,** 031802 (2013).
36. Jiang, C., Liu, H., Cui, Y. & Li, X. Electromagnetically induced transparency and slow light in two-mode optomechanics. *Opt. Express* **21,** 12165–12173 (2013).
37. Peng, B. *et al.* Parity-time-symmetric whispering-gallery microcavities. *Nat. Phys.* **10,** 394–398 (2014).
38. Yan, X. B. *et al.* Coherent perfect absorption, transmission, and synthesis in a double-cavity optomechanical system. *Opt. Express* **22,** 4886–4895 (2014).
39. Jing, H. *et al.* Optomechanically-induced transparency in parity-time-symmetric microresonators. *Sci. Rep.* **5,** 9663 (2015).
40. Xu, X. W. & Li, Y. Optical nonreciprocity and optomechanical circulator in three-mode optomechanical systems. *Phys. Rev. A* **91,** 053854 (2015).
41. Lei, F. C., Gao, M., Du, C. G., Jing, Q. L. & Long, G. L. Three-pathway electromagnetically induced transparency in coupled-cavity optomechanical system. *Opt. Express* **23,** 11508 (2015).
42. Lü, X. Y., Jing, H., Ma, J. Y. & Wu, Y. PT-symmetry-breaking chaos in optomechanics. *Phys. Rev. Lett.* **114,** 253601 (2015).
43. Gao, Y. J., Li, K., Nie, W. J. & Li, Y. Electromagnetically-induced-transparency-like ground-state cooling in a double-cavity optomechanical system. *Phys. Rev. A* **90,** 053841 (2014).
44. Liu, Y. C., Xiao, Y. F., Luan, X. S., Gong, Q. H. & Wong, C. W. Coupled cavities for motional ground-state cooling and strong optomechanical coupling. *Phys. Rev. A* **91,** 033818 (2015).
45. Zaks, B., Liu, R. B. & Sherwin, M. S. Experimental observation of electron-hole recollisions. *Nature* **483,** 580–583 (2012).
46. Huang, P., Xie, X. T., Lü, X. Y., Li, J. & Yang, X. Carrier-envelope-phase-dependent effects of high-order harmonic generation in a strongly driven two-level atom. *Phys. Rev. A* **79,** 043806 (2009).
47. Zhai, Z. *et al.* High-order harmonic generation with Rydberg atoms by using an intense few-cycle pulse. *Phys. Rev. A* **83,** 043409 (2011).
48. Li, J. H., Yu, R. & Wu, Y. Tunable higher-order sideband spectra in a waveguide-coupled photonic crystal molecule beyond the weak-excitation approximation. *Phys. Rev. A* **89,** 015802 (2014).
49. Li, J. H., Yu, R., Ding, C., Wang, W. & Wu, Y. Optical-frequency-comb generation and entanglement with low-power optical input in a photonic molecule. *Phys. Rev. A* **90,** 033830 (2014).
50. Krausz, F. & Ivanov, M. Attosecond physics. *Rev. Mod. Phys.* **81,** 163–234 (2009).
51. Wu, Y. & Yang, X. Carrier-envelope phase-dependent atomic coherence and quantum beats. *Phys. Rev. A* **76,** 013832 (2007).
52. Ding, L. *et al.* Wavelength-sized GaAs optomechanical resonators with gigahertz frequency. *Appl. Phys. Lett.* **98,** 113108 (2011).

Acknowledgements

Author Contributions

C.C., T.W. and C.W. wrote the main manuscript text, C.C. and C.W. prepared figures 1–5. All the authors reviewed the manuscript and discussed the results, drew conclusions and edited the manuscript.

Additional Information

Competing financial interests: The authors declare no competing financial interests.

How to cite this article: Cao, C. *et al.* Tunable high-order sideband spectra generation using a photonic molecule optomechanical system. *Sci. Rep.* **6,** 22920; doi: 10.1038/srep22920 (2016).